

Received October 23, 2020, accepted October 30, 2020, date of publication November 3, 2020, date of current version November 18, 2020.

Digital Object Identifier 10.1109/ACCESS.2020.3035653

Novel Hybrid Algorithm of Improved CKF and GRU for GPS/INS

DENGGAO LI^{1,3,4}, YUQI WU^{2,3,4}, AND JUMIN ZHAO^{2,3,4}

¹College of Data Science, Taiyuan University of Technology, Taiyuan 030024, China

²College of Information and Computer, Taiyuan University of Technology, Taiyuan 030024, China

³Technology Research Center of Spatial Information Network Engineering of Shanxi, Taiyuan 030024, China

⁴Shanxi Province Intelligent Perception Engineering Technology Center, Taiyuan 030024, China

Corresponding author: Denggao Li (lidenggao@tyut.edu.cn)

This work was supported in part by the National Key Research and Development Project (Broadband transceiver integrated devices and modules for data center applications) under Grant 2018YFB2200900, in part by the General Object of National Natural Science Foundation (Research on the key technology of BDS precision positioning in complex landform) under Grant 61772358, in part by the Transformation and Cultivation Project of Scientific and Technological Achievements of Universities in Shanxi Province (Disaster early warning system based on BDS high-precision positioning technology), and in part by the Key Technology Research and Development Program of Jinzhong (Deformation monitoring system integrating Beidou satellite positioning and 5G technology) under Grant Y201024.

ABSTRACT In order to ensure that Inertial Navigation System/Global Positioning System integrated navigation system (INS/GPS) can still provide high precision positioning results when GPS outages, a novel hybrid algorithm based on Gated Recurrent Unit (GRU) and interacting multiple model adaptive robust cubature Kalman filter (IMM-ARCKF) is proposed. Firstly, the IMM-ARCKF algorithm is proposed to solve the uncertainty of system model and measurement noise statics in the application of INS/GPS on the road. Then, GRU neural network is introduced into INS/GPS system which includes two modes of training and prediction. When GPS signal can be received, the GRU neural network works in the training mode. When GPS outages, the GRU neural network predicts the GPS position increment. Finally, the effectiveness of the algorithm is evaluated by the experiment and analysis. From the data of the experiment, the proposed algorithm can improve the positioning accuracy during GPS outages.


INDEX TERMS Integrated navigation, cubature Kalman filter, GPS outages, gated recurrent unit.

I. INTRODUCTION

The INS/GPS system has been used in more and more fields for its numerous advantages, especially in the military and civilian fields [1]. In terms of performance, GPS works well in long-term positioning. However, the GPS signal is easily blocked and the receiver positioning frequency is low. As an independent system, INS does not rely on external information when positioning, but its measurement error will accumulate over time during which more and more positioning errors will be produced in the integration calculation process. Therefore, the overall performance of INS/GPS integrated navigation system is far better than that of independent systems [2], [3].

At present, the data fusion algorithms commonly used in INS/GPS systems are Kalman Filter (KF) and Extended Kalman Filter (EKF) [4]. EKF is an improvement on the

traditional KF. EKF linearizes the state equation and the observation equation through first-order Taylor decomposition [5]. Both KF and EKF transform the problem into a linear Gaussian model, so the analytical form in the Bayesian recursive formula can be directly solved, which is convenient for calculation. As for the case of nonlinearity, EKF has the effect of linear error in addition to a large amount of calculation, so the Unscented Kalman filter (UKF) is proposed. UKF uses a series of determined samples to approximate the probability density distribution of a nonlinear function [6]. However, for the high-dimensional state model, the above filtering algorithms are prone to a non-positive definite covariance matrix [7]. Proposed by Arasaratnam *et al.*, Cubature Kalman filtering (CKF) is based on the third-order spherical radial volume criterion and uses a set of volume points to approximate the state mean and covariance of a nonlinear system with additional Gaussian noise. CKF is the closest approximation algorithm to Bayesian filtering in theory and is a powerful tool to solve nonlinear system state

The associate editor coordinating the review of this manuscript and approving it for publication was Kathiravan Srinivasan .

estimation [8], [9]. CKF has the same weight for each integral point, which is positive. Therefore, the numerical stability of CKF is stronger than that of UKF [10]. However, affected by the uncertainty of system model and the uncertainty of measurement noise statistics, the robustness is reduced and even the filter is failing. In recent years, many scholars have proposed many improved CKF algorithms to solve the above problems. Zhao *et al.* proposed an adaptive robust square root CKF algorithm based on the strong tracking filter principle and derived a suboptimal unbiased constant noise statistical estimator based on the maximum posterior principle [11]. To prevent the decrease of the positioning accuracy caused by the abnormal value in the measurement, Liu *et al.* used Huber M estimation technology to enhance the structure of the standard CKF [12]. Cui *et al.* proposed a robust Cubature Kalman filter (RCKF), which reused diffuse sigma points and approximate residuals in the prediction phase of CKF in the case of colored measurement noise and missing observed values [13]. Interactive multiple model is an effective method in maneuvering target tracking. The model can be combined with many algorithms to meet different application requirements [14], [15]. In literature [16], the fuzzy adaptive Kalman filtering (FAKF) algorithm and the adaptive interactive multiple model (AIMM) were combined to solve the problem that the prior information was inconsistent with the actual environment. Firstly, FAKF algorithm was used to calculate the rough statistical characteristics of noise. Secondly AIMM was used to determine the number of sub-filters according to the rough statistical characteristics. Finally, the localization results were solved. In literature [17], in order to improve the performance of SINS/DVL integrated navigation system, IMM-RKF algorithm was proposed. According to two different integrated navigation models, two different noise covariance is calculated. Then IMM algorithm was used to estimate the more real noise covariance matrix. The IMM-ARCKF algorithm can effectively solve the problem of measurement noise statistical characteristic inaccuracy in underwater environment.

Recently, artificial intelligence (AI) and big data have been applied in more extensive fields. Many scholars have applied AI methods to integrated navigation system, which can reduce the positioning error during GPS downtime [18]. In literature [19], multilayer feed-forward neural networks with a back propagation learning algorithm was used to fuse INS and DGPS data. Literature [20] proposed an ANN+GPS/INS system to solve the problem of large positioning error and fast drift caused by GPS signal loss in low-level GPS/INS systems. The system adopted multilayer perceptron structure neural network to construct the $O_{INS} - \Delta P$ module. The positioning accuracy was improved and the system drift was prevented effectively. In literature [21], a data fusion algorithm based on radial basis function neural network (RBFNN) was proposed which adopted $P_{INS} - \delta P$ structure. P_{INS} stood for INS position which was the input of the network. δP represented corresponding position error which was the output. Considering the relationship between INS error and

past value, input delay neural network (IDNN) was used in literature [22]. The algorithm modeled the error of INS position and velocity according to the current and past information of position and velocity. The network output was INS error. Literature [23] combined strong tracking Kalman filter (STKF) and wavelet neural network (WNN) algorithm. STKF was used to replace the traditional KF algorithm and WNN was used for training and prediction. The system used the $\delta P_{INS}(P) - \delta P_{INS}(C)$ structure. The past value of STKF was the input, and the current value was the expected output. When the GPS outages, trained WNN was used to replace STKF. In literature [24], a fusion algorithm based on back propagation neural network (BPNN) was proposed. The system adopted $O_{INS}T - \Delta P_{GPS}$ structure, and the model of the relationship between the speed of INS system, output of INS measurement unit and GPS fault duration and GPS position increment was established. In Literature [25], a dual optimization scheme was designed by combing CKF, MLP and RBF. Firstly, CKF was added to MLP as an optimizer, which can adaptively estimate the weight of MLP. Then, RBF and CKF were used for error estimation. In reference [26], to improve the navigation accuracy, the regression fuzzy wavelet neural network (RFWNN) was added to the INS/GPS system to compensate the speed and position errors of INS/GPS. Most of the neural networks mentioned above, such as RBF and MLP, belong to static networks. The main disadvantage of these networks is that they only use information from the last step and cannot store more information in the past. Since GRU is used for events related to time series, we use GRU for INS/GPS system.

The interacting multiple model robust adaptive cubature Kalman filter based on GRU (GRU/IMM-ARCKF) is proposed. When GPS signal acquisition is normal, the fusion algorithm uses the IMM-ARCKF algorithm and the GRU is trained at the same time. When GPS signals cannot be obtained normally, GRU is used to predict GPS position increment. The pseudo GPS position is obtained by integrating the position increment.

Other parts are as follows: Section II derives the traditional CKF algorithm and the proposes IMM-ARCKF algorithm; Section III discusses the GRU-aided integrated navigation algorithm; In section IV, the simulation results and experimental results are analyzed. Finally, the conclusion is given.

II. IMM-ARCKF

When the system model error and noise statistical error exist in high dynamic scene, the traditional CKF algorithm is easy to make the positioning error larger. To overcome the uncertainty of measurement noise statistics, Huber M-estimation is adopted to allow the measurement noise covariance to be automatically adjusted. To overcome the error of the system model, an adaptive factor is used to adjust the state covariance matrix. When the GPS/INS system is applied in actual scenarios, the above two uncertainties will exist simultaneously. Therefore, interacting multiple model is used to combine RCKF and ACKF. According to the information of each

sub-filter, such as the covariance of the innovation matrix, the mode probability of each sub-filter is calculated. Finally, the state estimation of ACKF and RCKF are weighted by probability to obtain the final state estimation. IMM-ARCKF not only overcomes partial limitations of traditional CKF, but also combines the advantages of ACKF and RCKF to improve the adaptability and robustness of the system.

A. TRADITIONAL CKF

In actual applications, INS is generally not used alone. Its measurement error will accumulate with time, eventually leading to divergence of positioning results. Therefore, IMM-ARCKF is proposed to optimize the combination of GPS and INS system. The linear error equation of INS is [27]:

$$\dot{\phi}^n = -\omega_{in}^n \times \phi + \delta\omega_{in}^n - C_b^n \delta\omega_{ib}^b \tag{1}$$

$$\delta\dot{v}^n = C_b^n \delta f^b + C_b^n f^b \times \phi - (2\omega_{ie}^n + \omega_{en}^n) \times \delta v^n + \delta g^n \tag{2}$$

$$\delta\dot{L} = \frac{1}{R_M + h} \delta v_N \tag{3}$$

$$\delta\dot{\lambda} = \frac{1}{(R_M + h) \cos L} \delta v_E + \frac{V_E \tan L}{(R_N + h) \cos L} - \frac{\delta h V_E}{(R_N + h)^2 \cos L} \tag{4}$$

$$\delta\dot{h} = \delta v_u \tag{5}$$

where δL and $\delta\lambda$ represent the error of longitude and latitude, and δh represents the error of altitude. The superscript 'n' represents the navigation frame (N-frame), and the subscript 'e' represents the earth frame (e-frame). ω_{ie}^n is the rotation rate of the earth, and $\delta\omega_{ie}^n$ is its error. ϕ stands for misalignment angle vector. C_b^n is the direction cosine matrix.

The traditional CKF is as follows. Nonlinear dynamic equation:

$$x_k = f(x_{k-1}) + w_{k-1} \tag{6}$$

$$z_k = h(x_k) + v_k \tag{7}$$

where x_k represents the state vector of m dimension in the k epoch; z_k stands for n dimensional measurement; w_{k-1} is the system noise. Its mean is 0. Its covariance is Q_{k-1} ; v_k stands for measurement noise whose mean is 0. And its covariance is R_k ; $f(\cdot)$ and $h(\cdot)$ represent nonlinear equation of state and system measurement equation respectively.

Time Update:

(1) Decomposition

$$P_{k|k-1} = S_{k-1|k-1} S_{k-1|k-1}^T \tag{8}$$

(2) Generating cubature points

$$X_{i,k|k}^h = S_{k-1|k-1} \xi_i + \hat{x}_{k-1|k-1} \tag{9}$$

$$\xi = \begin{cases} \sqrt{m e_i}, & i = 1, 2, \dots, m \\ \sqrt{m e_{n-i}}, & i = m + 1, m + 2, \dots, 2m \end{cases} \tag{10}$$

where m is the number of basic cubature points.

(3) Propagation cubature points

$$X_{i,k-1|k-1}^* = f\left(X_{i,k-1|k-1}^h\right) \tag{11}$$

(4) Predicted states

$$\hat{x}_{k|k-1} = (2m)^{-1} \sum_{i=1}^{2m} X_{i,k-1|k-1}^* \tag{12}$$

(5) Predicted state error covariance

$$P_{k|k-1} = (2m)^{-1} \sum_{j=1}^{2m} X_{i,k-1|k-1}^* X_{i,k-1|k-1}^{*T} - \hat{x}_{k|k-1} \hat{x}_{k|k-1}^T + Q_{k-1} \tag{13}$$

Measurement update

(1) Decomposition

$$P_{k|k-1} = S_{k|k-1} S_{k|k-1}^T \tag{14}$$

(2) Generating cubature points

$$X_{i,k|k-1} = S_{k|k-1} \xi_i + \hat{x}_{k|k-1} \tag{15}$$

(3) Propagation cubature points

$$Z_{i,k-1|k-1}^* = h\left(X_{i,k|k-1}\right) \tag{16}$$

(4) Predicted measurement

$$\hat{z}_{k|k-1} = (2m)^{-1} \sum_{i=1}^{2m} Z_{i,k-1|k-1}^* \tag{17}$$

(5) Innovation covariance

$$P_{k|k-1}^{zz} = (2m)^{-1} \sum_{i=1}^{2m} Z_{i,k|k-1}^* Z_{i,k|k-1}^{*T} - \hat{z}_{k|k-1} \hat{z}_{k|k-1}^T + R_k \tag{18}$$

(6) Cross-covariance matrix

$$P_{k|k-1}^{xz} = (2m)^{-1} \sum_{i=1}^{2m} X_{i,k|k-1}^* h Z_{i,k|k-1}^{*T} - \hat{x}_{k|k-1} \hat{z}_{k|k-1}^T \tag{19}$$

(7) Kalman gain

$$G_k = P_{k|k-1}^{xz} \left(P_{k|k-1}^{zz}\right)^{-1} \tag{20}$$

(8) Updating the state

$$\hat{x}_{k|k} = \hat{x}_{k|k-1} + G_k \left(z_k - \hat{z}_{k|k-1}\right) \tag{21}$$

(9) Updating the state covariance matrix

$$P_{k|k} = P_{k|k-1} - G_k P_{k|k-1}^{zz} G_k^T \tag{22}$$

B. ROBUST CKF

In dynamic systems, large observation errors are inevitable. The on-line adaptive adjustment ability of the system is very important. Robust M estimation can be used for adaptive estimation of unknown prior states and measurements [28]. The expression in the measurement update process is updated as:

$$\bar{P}_{k|k-1}^{zz} = (2m)^{-1} \sum_{i=1}^{2\pi} Z_{i,k|k-1}^* Z_{i,k|k-1}^{*T} - \hat{z}_{k|k-1} \hat{z}_{k|k-1}^T + \bar{R}_k \tag{23}$$

where \bar{R}_k is the adjusted R_k . \bar{R}_k can be calculated from equal weight matrix \bar{H} using contrast M estimation method.

$$\bar{R}_k = \bar{H}^{-1} \quad (24)$$

To ensure that the diagonal elements of \bar{H} are positive, we use Huber method to calculate \bar{H} .

$$\bar{h}_{ii} = \begin{cases} 1/\delta_{ii} & |v_i/\delta_{v_i}| = |v'_i| \leq c \\ c/\delta_{ii} |v'_i| & |v'_i| > c \end{cases} \quad (25)$$

$$\bar{h}_{ij} = \begin{cases} 1/\delta_{ij} & |v'_i| \leq c \text{ and } |v'_j| \leq c \\ \frac{c}{\delta_{ij} \max\{|v'_i|, |v'_j|\}} & |v'_i| > c \text{ or } |v'_j| > c \end{cases} \quad (26)$$

where \bar{h}_{ii} is the diagonal element of \bar{H} , and \bar{h}_{ij} is the off-diagonal element. δ_{ii} is the diagonal element of R_k , and δ_{ij} is the off-diagonal element of R_k .

$$\delta_{v_i} = \left(P_{k|k-1}^{zz} \right)_{ii} \quad (27)$$

where c is a constant, between 1.3 and 2.0. Robust CKF algorithm alleviates the impact of statistical uncertainty of measurement noise on system performance. The real-time adjustment of measurement noise statistics is realized.

C. ADAPTIVE CKF

When the error of the dynamic model in a integrated navigation system is large compared with the real model, it may affect all state estimation results. Adaptive adjustment factors were used to modify the state error covariance [29]:

$$\begin{aligned} P'_{k|k-1} &= \omega_k^{-1} P_{k|k-1} \\ &= \omega_k^{-1} \left[(2m)^{-1} \sum_{j=1}^{2m} X_{i,k-1|k-1}^* X_{i,k-1|k-1}^{*T} \right. \\ &\quad \left. - \hat{x}_{k|k-1} \hat{x}_{k|k-1}^T + Q_{k-1} \right] \end{aligned} \quad (28)$$

where ω_k is the adaptive factor which is derived as follows.

Calculate the predicted residual vector:

$$e_k = z_k - \hat{z}_{k|k-1} \quad (29)$$

The theoretical predicted covariance matrix of residual vector e_k is:

$$\begin{aligned} P_{k|k-1}^{zz} &= E \left((z_k - \hat{z}_{k|k-1}) (z_k - \hat{z}_{k|k-1})^T \right) \\ &= D_k P_{k|k-1} D_k^T + R_k \end{aligned} \quad (30)$$

where $D_k = \frac{\partial h(x_k)}{\partial x_k}$. Then the adaptive factor are substituted in:

$$P_{k|k-1}^{zz'} = \omega_k^{-1} D_k P_{k|k-1} D_k^T + R_k \quad (31)$$

Assuming that the estimated covariance matrix of the prediction residual vector is $P_{k|k-1}^{zz''}$. The value of the adaptive factor should meet the following equation:

$$P_{k|k-1}^{az'} = P_{k|k-1}^{vz''} \quad (32)$$

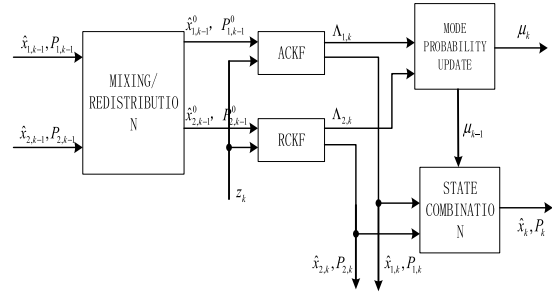


FIGURE 1. Flow chart of IMM-ARCKF algorithm.

Continue derivation:

$$P_{k|k-1}^{zz'} = \omega_k^{-1} D_k P_{k|k-1} D_k^T + R_k \quad (33)$$

Multiply both sides by ω_k :

$$\omega_k P_{k|k-1}^{zz''} = D_k P_{k|k-1} D_k^T + \omega_k R_k \quad (34)$$

$$\omega_k \left(P_{k|k-1}^{zz''} - R_k \right) = D_k P_{k|k-1} D_k^T \quad (35)$$

$$\begin{aligned} \omega_k &= \frac{\text{tr} \left(D_k P_{k|k-1} D_k^T \right)}{\text{tr} \left(P_{k|k-1}^{zz''} - R_k \right)} \\ &= \frac{\text{tr} \left(P_{k|k-1}^{zz} - R_k \right)}{\text{tr} \left(P_{k|k-1}^{zz''} - R_k \right)} \end{aligned} \quad (36)$$

Since $0 < \omega_k \leq 1$ [30], the value of ω_k is as follows:

$$\omega_k = \begin{cases} 1 & \text{otherwise} \\ \frac{\text{tr} \left(D_k P_{k|k-1} D_k^T \right)}{\text{tr} \left(P_{k|k-1}^{zz''} - R_k \right)} = \frac{\text{tr} \left(P_{k|k-1}^{zz''} - R_k \right)}{\text{tr} \left(P_{k|k-1}^{zz''} - R_k \right)} & \text{tr} \left(P_{k|k-1}^{zz''} \right) \\ & > \text{tr} \left(P_{k|k-1}^{zz} \right) \end{cases} \quad (37)$$

R_k exists in both numerator and denominator of the above formula. Then the approximate optimal adaptive factor calculated as follows:

$$\omega_k = \begin{cases} 1 & \text{otherwise} \\ \frac{\text{tr} \left(P_{k|k-1}^{zz''} \right)}{\text{tr} \left(P_{k|k-1}^{zz''} \right)} & \text{tr} \left(P_{k|k-1}^{zz''} \right) > \text{tr} \left(P_{k|k-1}^{zz} \right) \end{cases} \quad (38)$$

D. IMM-ARCKF

From the above analysis, it can be concluded that RCKF mainly alleviates the impact of measurement noise statistical uncertainty while ACKF mainly alleviates the impact of system model error uncertainty. Therefore, IMM fusion algorithm is used to combine ACKF and RCKF. The flow chart is as follows:

In the proposed IMM-ARCKF algorithm, ACKF filter and RCKF filter run in parallel. And the two filters have different models. Then the model probability is calculated based on the measurement error covariance matrix of ACKF and RCKF.

Finally, the state results of ACKF filter and RCKF filter are fused.

1) INITIALIZATION

Markov transition matrix and probability of initial mode are:

$$A = \begin{bmatrix} a_{11} & a_{12} \\ a_{21} & a_{22} \end{bmatrix}, \theta_0 = \begin{bmatrix} \theta_{1,0} \\ \theta_{2,0} \end{bmatrix} \quad (39)$$

where a_{ij} is the transfer probability. θ_0 is the mode probability, which describes the reliability probability of each sub-filter at the current moment. And meet $\theta_{1,0} + \theta_{2,0} = 1$.

2) UPDATE MODEL PROBABILITY

The model probability is an important index to fuse the state estimation results of subfilters.

$$\theta_{j,k} = \frac{\Lambda_{j,k} d_{j,k-1}}{\sum_{j=1}^2 \Lambda_{j,k} d_{j,k-1}} \quad (40)$$

where $\Lambda_{j,k}$ is the likelihood function. d is the normalization factor, calculated as follows:

$$d_0 = A^T \theta_0 = [d_{1,0} \quad d_{2,0}] \quad (41)$$

$$\Lambda_{j,k} = \frac{1}{\sqrt{(2\pi)^n |P_{\hat{z}_{k/k-1}}^{zz,j}|}} \exp \left\{ -\frac{1}{2} e_{j,k}^T \left(P_{\hat{z}_{k/k-1}}^{zz,i} \right)^{-1} e_{j,k} \right\} \quad (42)$$

$P_{\hat{z}_{k/k-1}}^{zz,j}$ is calculated as follows:

$$P_{\hat{z}_{k|k-1}}^{zz,1} = (2m)^{-1} \sum_{i=1}^{2m} \left(Z_{i,k|k-1}^{*1} - \hat{z}_{k|k-1}^1 \right) \times \left(Z_{i,k|k-1}^{*1} - \hat{z}_{k|k-1}^1 \right)^T + R_k \quad (43)$$

$$P_{\hat{z}_{k|k-1}}^{zz,2} = (2m)^{-1} \sum_{i=1}^{2m} \left(Z_{i,k|k-1}^{*2} - \hat{z}_{k|k-1}^2 \right) \times \left(Z_{i,k|k-1}^{*2} - \hat{z}_{k|k-1}^2 \right)^T + \bar{R}_k \quad (44)$$

where $P_{\hat{z}_{k|k-1}}^{zz,1}$ is the innovation covariance matrix in ACKF filter. $P_{\hat{z}_{k|k-1}}^{zz,2}$ is the innovation covariance matrix of RCKF filter.

From the above derivation, it can be seen that the smaller the innovation matrix is, the more the subfilter corresponds to the actual system, and the larger $\Lambda_{j,k}$ will be. Therefore, the value of θ_0 corresponding to the subfilter is larger. When the error of process model is larger than the statistical error of measurement noise, the model probability of ACKF is larger. Conversely, when the error of measurement noise statistics is greater than the error of the process model, the modal probability of RCKF is larger.

3) REDISTRIBUTION

$\hat{x}_{j,k}$ and $P_{j,k}$ are redistributed and then used as the initial value of the sub-filter at the next moment.

$$\hat{x}_{i,k}^0 = \sum_{j=1}^2 \hat{x}_{j,k} h_{ij,k} \quad (45)$$

$$P_{i,k}^0 = \sum_{j=1}^2 \left\{ P_{j,k} + [\hat{x}_{j,k} - \hat{x}_{i,k}^0] [\hat{x}_{j,k} - \hat{x}_{i,k}^0]^T \right\} h_{ij,k} \quad (46)$$

where $i = 1,2$; $h_{ij,k}$ is the mixed probability.

$$h_{ij,k} = \frac{a_{ij} \theta_{j,k}}{d_{i,k}}, \quad h_{1j,k} + h_{2j,k} = 1 \quad (47)$$

4) THE FUSION RESULTS

Through the calculated model probability and the estimated state results of the two sub-filters, the final state estimation fusion is performed:

$$\hat{x}_k = \sum_{j=1}^2 \hat{x}_{j,k} \theta_{j,k} \quad (48)$$

$$P_k = \sum_{j=1}^2 \left\{ P_{j,k} + [\hat{x}_{j,k} - \hat{x}_k] [\hat{x}_{j,k} - \hat{x}_k]^T \right\} \theta_{j,k} \quad (49)$$

5) FLOW OF IMM-ARCKF ALGORITHM

a Initialization

The initialization of A, θ_0 can be done by formula (39). Then the ACKF filter and RCKF filter are initialized to obtain the $\hat{x}_{i,k}^0$ and $P_{i,k}^0$ of each filter

b ACKF and RCKF run in parallel

ACKF and RCKF reduce the impact of uncertainty of system model and uncertainty of measurement noise statistics on filtering performance respectively. Their respective models are different. ACKF and RCKF run in parallel, and then the state of each subfilter and corresponding error covariance matrix are obtained.

c Multifilter fusion

According to Equations (48)-(49), the final estimation result of IMM-ARCKF algorithm is calculated.

d Repeat steps b and c until the positioning is complete.

III. GRU-DIDED THE INS/GPS

A. GATED RECURRENT UNIT

If we deal with problems related to the timeline of events, such as pedestrian trajectory prediction, vehicle trajectory prediction, natural language processing, text processing, etc., traditional neural networks are unable to perform it. It is therefore proposed that recurrent neural network (RNN) [31]. GRU control process is similar to RNN. Both of them process data flowing through cells during forward propagation. The difference is that the structure and operation of cells in GRU are different from that in RNN [32]. GRU is a variant of the Long-Term Memory (LSTM) that merges the input gates and forgetting gates, and merges the memory state and the hidden

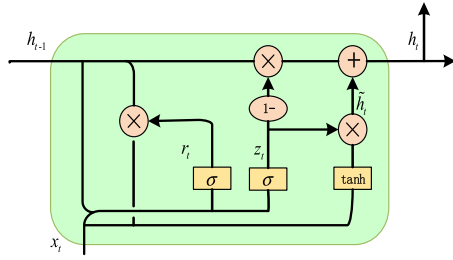


FIGURE 2. The GRU module.

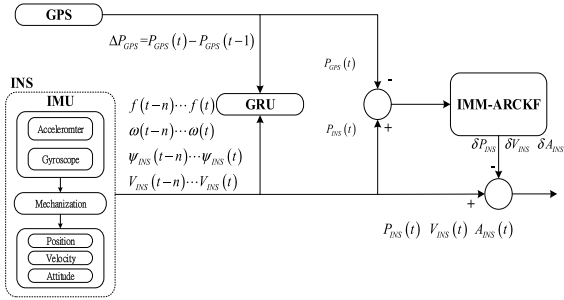


FIGURE 3. The training phase.

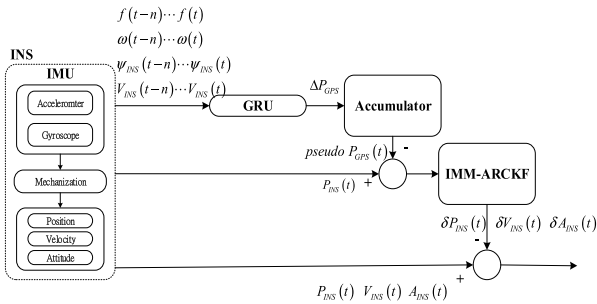


FIGURE 4. The predicting phase.

state. GRU has much fewer parameters than LSTM, and the training speed is faster [33]. The hidden layer unit in the GRU neural network introduces a gating unit, and its structure is as follows [34]:

The calculation process is as follows:

$$z_t = \sigma(W_z \cdot [h_{t-1}, x_t]) \quad (50)$$

$$r_t = \sigma(W_r \cdot [h_{t-1}, x_t]) \quad (51)$$

$$\tilde{h}_t = \tanh(W \cdot [r_t^* h_{t-1}, x_t]) \quad (52)$$

$$h_t = (1 - z_t)^* h_{t-1} + z_t^* \tilde{h}_t \quad (53)$$

In the figure z_t and r_t represent update and reset gates respectively. The greater the value of the update gate, the more information was brought in from the previous moment. The smaller the value of the reset door, the less information from the previous moment was written.

B. GRU-ADIED INS/GPS

In this article, GRU is applied to INS/GPS integrated navigation system and $O_{INS} - \Delta P$ structure is proposed. As shown

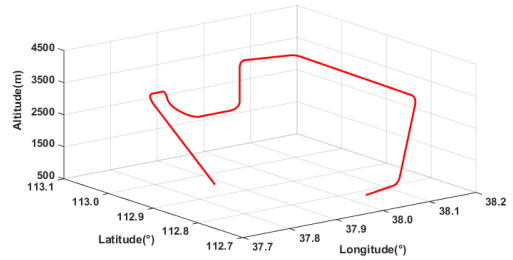


FIGURE 5. Simulated flight trajectory.

in Figure (3) and (4). When the GPS signal is properly acquired, the GRU is trained. In this stage, INS and GPS information are fused through IMM-ARCKF to obtain positioning results. In addition, the yaw angle ψ_{INS} and velocity V_{INS} of INS and the angular velocity ω and specific force f of IMU are taken as input, and the output is the position increment of GPS. When GPS signals cannot be obtained, GRU is used for prediction. The ψ_{INS} , V_{INS} , ω and f are input into the trained GRU to obtain the predicted GPS increment. The pseudo GPS position is obtained after integrating this value, and then it is sent to IMM-ARCKF.

It is worth noting that the neural network not only uses the information of the previous one-step, but also takes $\{x(t-3)x(t-2)x(t-1)x(t)\}$ as the input.

IV. PERFORMANCE EVALUATION

A. PERFORMANCE VERIFICATION OF IMM-ARCKF

In this section, IMM-ARCKF is compared with the classical CKF, ACKF and RCKF through numerical simulation experiments and on-board experiments to verify the effectiveness of the IMM-ARCKF. The root mean square error (RMSE) is used as a metric to compare the performance of these algorithms and verify the effectiveness of the proposed algorithm. We performed 50 independent Monte Carlo simulations for performance comparisons.

E-N-U geographic coordinate system is adopted for INS/GPS integrated navigation system. INS/GPS integrated navigation process model is composed of INS mechanical calibration equation and inertial sensor error equation. The system state vector is defined as:

$$x(t) = [\varphi_E \ \varphi_N \ \varphi_U \ \delta v_E \ \delta v_N \ \delta v_U \ \delta L \ \delta \lambda \ \delta h \ \varepsilon_x \ \varepsilon_y \ \varepsilon_z \ \nabla_x \ \nabla_y \ \nabla_z] \quad (54)$$

where, $(\varphi_E \ \varphi_N \ \varphi_U)$ represent the attitude Angle error; $(\delta v_E \ \delta v_N \ \delta v_U)$ stand for velocity error; $(\delta L \ \delta \lambda \ \delta h)$ stand for position error; $(\varepsilon_x \ \varepsilon_y \ \varepsilon_z)$ stand for gyro constant drift; $(\nabla_x \ \nabla_y \ \nabla_z)$ stand for accelerometer constant drift.

The observation vector is:

$$z = \begin{bmatrix} v_{gps}^E - v_{ins}^E & v_{gps}^N - v_{ins}^N & v_{gps}^U - v_{ins}^U \\ L_{gps} - L_{ive} & \lambda_{gps} - \lambda_{ins} & h_{gps} - h_{ins}^T \end{bmatrix} \quad (55)$$

The discretized state equation is:

$$X_k = \phi_{k,k-1} X_{k-1} + W_{k-1} \quad (56)$$

TABLE 1. The simulation initialization parameters.

Initial position	East longitude	37.7050°
	North latitude	112.7196°
	Altitude	500m
Initial velocity	East	0 m/s
	North	0m/s
	Up	150m/s
Initial attitude	Pitch	0°
	Roll	0°
	Yaw	0°
Initial velocity error	East	0.4 m/s
	North	0.3 m/s
	Up	0.4 m/s
Initial position error	East longitude	12m
	North latitude	12m
	Altitude	15m
Initial attitude error	Yaw	1.5'
	Pitch	1'
	Roll	1.5'
Gyro parameters	Constant drift	0.1°/h
	Random walk coefficient	0.05 °/ \sqrt{h}
	Sampling frequency	20Hz
	Zero-bias	1 × 10 ⁻³ g
Accelerometer parameters	Random walk coefficient	1 × 10 ⁻⁴ g × \sqrt{s}
	Sampling frequency	20Hz
Initial Marcov Transition matrix	$A = \begin{bmatrix} 0.4 & 0.6 \\ 0.6 & 0.4 \end{bmatrix}$	
Initial mode probability	$\theta_0 = \begin{bmatrix} 0.4 \\ 0.6 \end{bmatrix}$	

The observation equation is:

$$z_k = H_k x_k + v_k \quad (57)$$

where $H_k = [0_{6 \times 3} I_{6 \times 6} 0_{6 \times 6}]$ and v_k is the measurement noise matrix.

1) SIMULATION AND ANALYSIS

Assume that the fixed-wing aircraft performs maneuverable flight, which consists of various actions. In Figure (5),

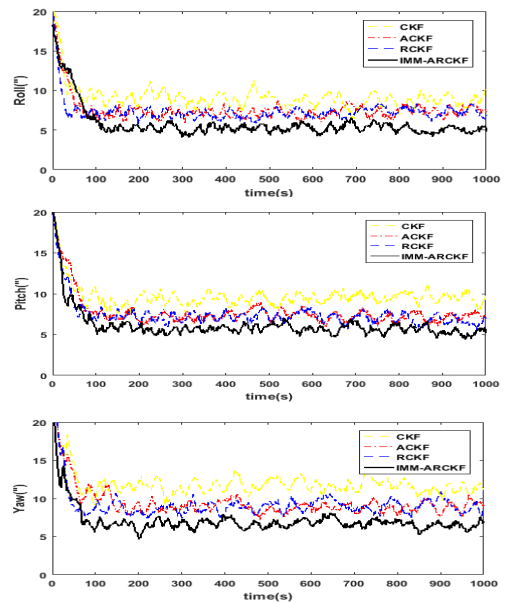


FIGURE 6. Attitude RMSEs by CKF, ACKF, RCKF and IMM-ARCKF for the simulation case.

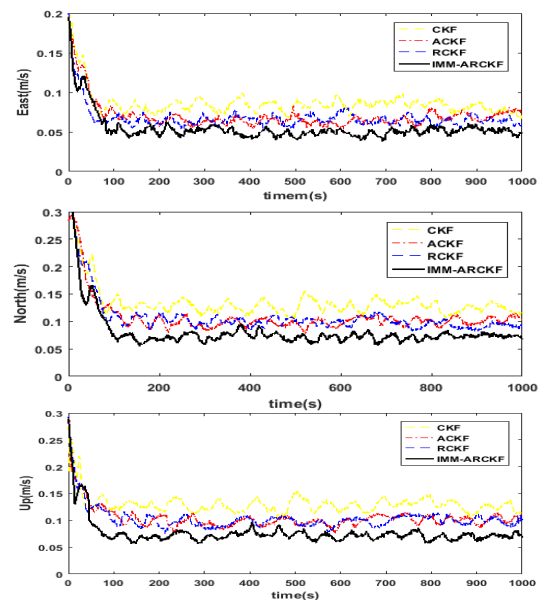


FIGURE 7. Velocity RMSEs by CKF, ACKF, RCKF and IMM-ARCKF for the simulation case.

the flight path of the aircraft is designed. Table 1 is the simulation parameter. The filtering cycle is 1s and the simulation time is 1000s.

The following is the comparative simulation results of a Monte Carlo (MC) run. Figure (6) depicts the attitude RMSE of CKF, ACKF, RCKF and IMM-ARCKF in a Monte Carlo simulation. From the figure, the attitude RMSE of ACKF, RCKF and the IMM-ARCKF are all smaller than the classical CKF within 100 to 1000 seconds. The attitude RMSE of IMM-ARCKF is the smallest. Figure (7) and figure (8) are the velocity RMSE and position RMSE

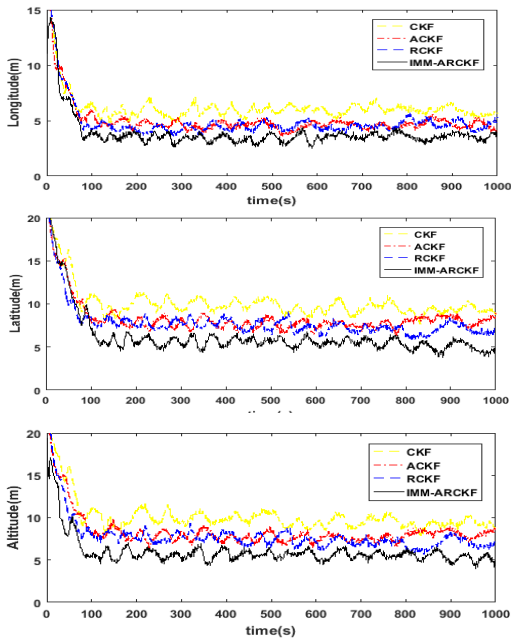


FIGURE 8. Position RMSEs by CKF, ACKF,RCKF and IMM-ARCKF for the simulation case.

TABLE 2. The mean root mean square errors of CKF, RCKF, ACKF and IMM-ARCKF in attitude, velocity and position.

		CKF	ACKF	RCKF	IMM-ARCKF
Attitude ($^{\circ}$)	Yaw	11.6019	9.0620	8.8719	6.6628
	Pitch	9.3725	7.2801	7.1317	5.6938
	Roll	8.8766	7.2542	7.1273	5.2618
Velocity (m/s)	East	0.0827	0.0662	0.0650	0.0504
	North	0.1269	0.0994	0.0991	0.0721
	Up	0.1272	0.1021	0.0991	0.0721
Position (m)	Longitude	5.9053	4.6587	4.4839	3.4925
	latitude	9.6435	7.8424	7.3763	5.4548
	Altitude	9.6221	7.8220	7.3672	5.4560

obtained by CKF,, ACKF, RCKF and IMM-ARCKF in a Monte Carlo simulation. The velocity error and position error trends of the above four methods are similar to the attitude error, among which the velocity and position error of the IMM-ARCKF is much smaller than that of the other methods. Table 2 lists the RMSEs of attitude, velocity and position of CKF, ACKF, RCKF and IMM-ARCKF in a Monte Carlo simulation. The positioning accuracy of the IMM-ARCKF is at least 40.1% higher than that of the classical CKF.

Simulation results show that IMM-ARCKF in this article can well combine the advantages of ACKF and RCKF, thus significantly improving the navigation accuracy of INS/GPS integration.

Figure (9) - Figure (11) shows the average RMSE of 50 Monte Carlo calculations. It can be seen that

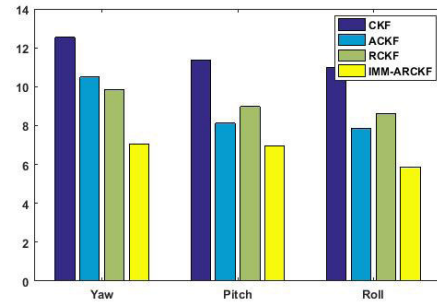


FIGURE 9. Mean of attitude RMSE for 50 Monte Carlo simulations.

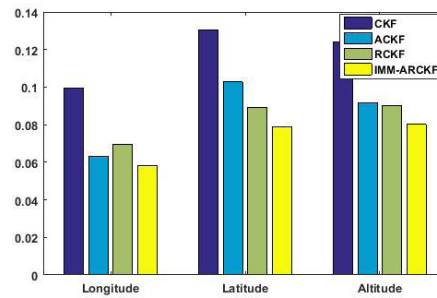


FIGURE 10. Mean of velocity RMSE for 50 Monte Carlo simulations.

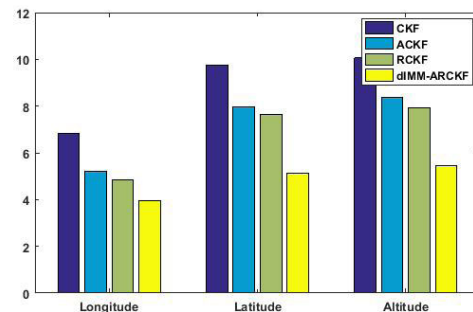


FIGURE 11. Mean of position RMSE for 50 Monte Carlo simulations.

IMM-ARCKF has high precision, and shows better stability and robustness compared with the standard CKF algorithm and RCKF algorithm.

2) THE FIRST EXPERIMENT AND ANALYSIS

As shown in figure (12), the vehicle is equipped with an INS/GPS integrated navigation system. The experimental instruments include the iN5620 integrated navigation receiver and I50 small intelligent RTK receiver.

The vehicle trajectory is shown in figure (13). The vehicle navigation test was conducted in Jinzhong city, Shanxi Province. The initial position was at North latitude $37^{\circ}44'44.4''$, East longitude $112^{\circ}42'07.3''$. The horizontal position error of GPS receiver is 4m. The height error is 7m, and the speed error is 0.05 m/s. The test time is 1000s and the filtering period is 1s. The initial velocities of east, north, and up are 10m/s, 10m/s, and 0m/s, respectively. The gyroscopic constant drift is $0.1^{\circ}/h$. The accelerometer zero bias is $10^{-3}g$.

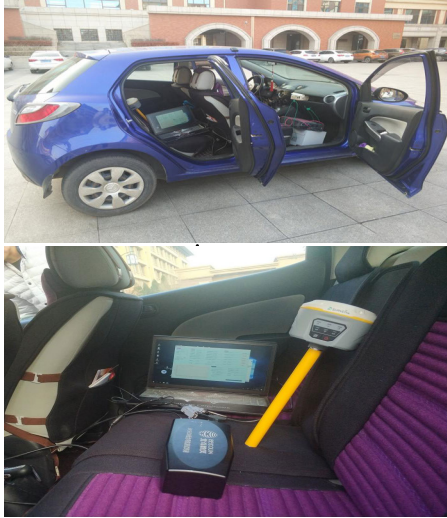


FIGURE 12. Test vehicle with equipment.

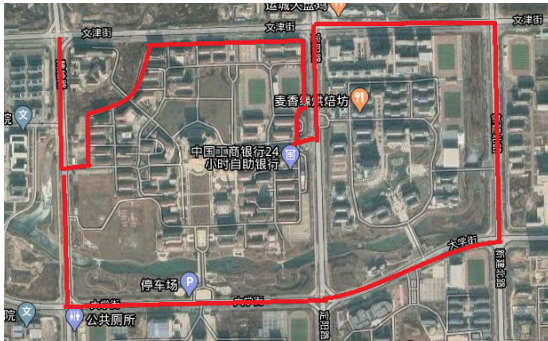


FIGURE 13. The vehicle trajectory of the first test.

The initial position error of the vehicle is (12m, 12m, 15m). The initial speed error is (0.3m/s, 0.4m/s, 0.3m/s), and the initial attitude error is (1', 1.5', 1').

Figure (14) and figure (15) respectively depict the longitude and latitude errors of the classical CKF, ACKF, RCKF and the IMM-ARCKF in the on-board experiment. Within 100s to 1000s, the longitude error of classical CKF is between (-24.9m,25.0m) and latitude error is between (-25.0m,20.0m). ACKF and RCKF improve the positioning accuracy to some extent. The longitude error of the proposed IMM-ARCKF algorithm is within (-5.3m, 5.1m), and the latitude error is between (-5.5m, 5.2m). The longitude and latitude error of IMM-ARCKF algorithm is much smaller than that of classical CKF,ACKF and RCKF. Therefore, IMM-ARCKF has stronger adaptability and robustness, and higher navigation accuracy.

Table 3 shows the mean root mean square error of longitude and latitude of CKF, RCKF, ACKF and IMM-ARCKF. It can be seen that the positioning accuracy of IMM-ARCKF is obviously better than that of traditional CKF algorithm.

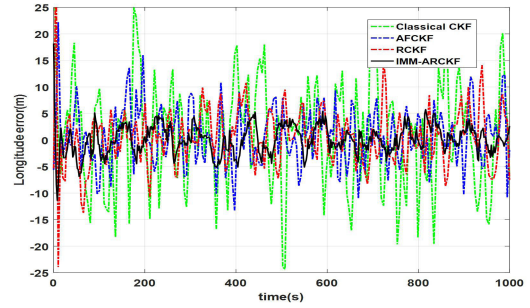


FIGURE 14. Longitude error.

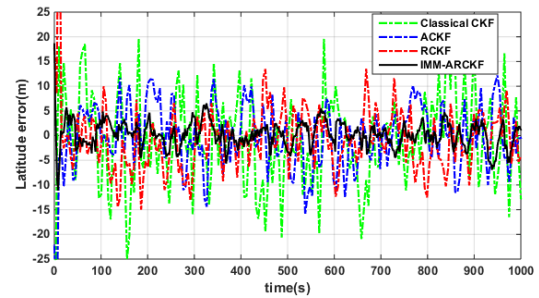


FIGURE 15. Latitude error.

TABLE 3. The mean root mean square errors of CKF, RCKF, ACKF and IMM-ARCKF in Longitude and latitude.

	CKF	ACKF	RCKF	IMM-ARCKF
Longitude (m)	9.1113	5.9753	5.0811	3.5948
Latitude (m)	8.4930	5.5030	6.2807	3.6497



FIGURE 16. The vehicle trajectory of the second test.

B. GRU-/IMM-ARCKF COMPARED WITH OTHER ALGORITHM

The training of neural network needs a lot of data, so the distance of this experiment is long. The experimental trajectory is shown in Figure (16). The black part is the process of artificial outages. When the GPS receiver is working normally, the system is in loose coupling mode and GRU is trained. When GPS is interrupted artificially, GRU makes prediction and outputs the INCREMENT of GPS. The whole process took 3,000 seconds.

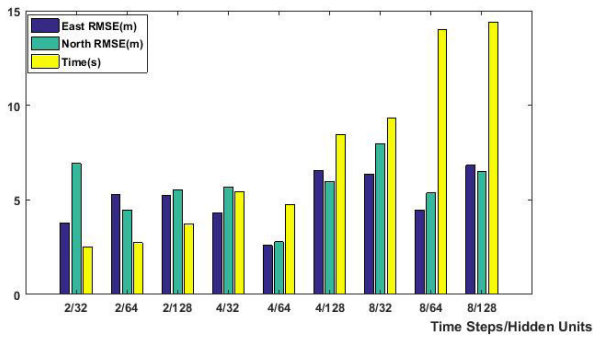


FIGURE 17. Performance comparison of different parameter.

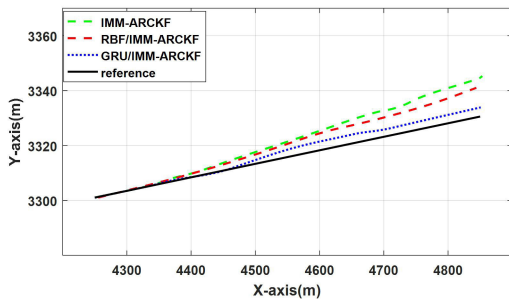


FIGURE 18. Positioning results in 60s outages.

1) PARAMETER TRAINING OF GRU

The model was designed to consist of two GRU layers and a full connection layer activated by the SOFTMAX function. The learning rate was set at 0.001. Using the RMSE as the criterion for selecting parameters. In practice, we usually evaluate the generalization ability of learning methods by testing errors. When training the GRU, we need to determine the parameters such as the number of hidden units and the time step size. If it is too much, it will consume a lot of time and real time performance degradation. Based on the RMSE, the performance of several time step sizes and the number of hidden units is evaluated. To select the appropriate parameters. Figure (17) shows the performance differences of different parameters.

It can be intuitively seen that when the step size is 4 and the hidden cell is 64, the RMSE in each direction is lower, so this combination is selected.

2) THE SECOND EXPERIMENT AND ANALYSIS

To evaluate the overall performance of the GRU/IMM-ARCKF, an actual road experiment is carried out after the parameters are selected. During the experiment, three segments were set up for 60 seconds, 100 seconds and 200 seconds respectively. And compared with the algorithm IMM-ARCKF, RBF/IMM-ARCKF and the proposed algorithm.

Figure (18) is positioning results figure in 60s outages. The black line in the figure is the reference trajectory. The green one represents the traditional IMM-ARCKF

TABLE 4. The error comparison of several algorithms when GPS outages.

Algorithm	IMM-ARCKF		RBF /IMM-ARCKF		GRU /IMM-ARCKF	
	Max	Mean	Max	Mean	Max	Mean
#1	56.98	27.57	35.06	19.69	17.83	6.68
#2	138.11	98.56	61.92	24.46	25.61	13.72
#3	351.38	201.86	241.59	130.74	58.26	20.16

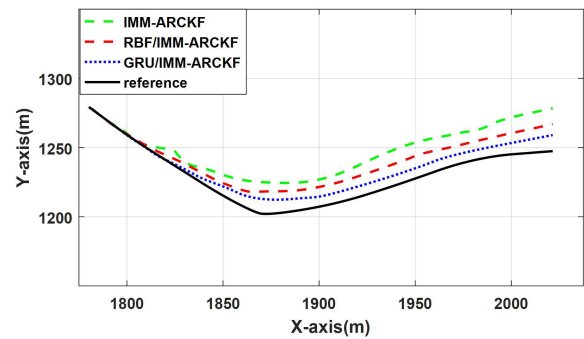


FIGURE 19. Positioning results in 100s outages.

algorithm. The red one represents the RBF/IMM-ARCKF, and the blue one represents the proposed GRU/IMM-ARCKF. In Figure (18), the positioning error of each algorithm increases with the increase of time during GPS interruption. But the error increase of each algorithm is obviously different. The position error of IMM-ARCKF increases the fastest while that of GRU/IMM-ARCKF is the slowest. Compared with IMM-ARCKF and RBF/IMM-ARCKF, the GRU/IMM-ARCKF has higher positioning accuracy. Table 4 shows that the maximum positioning error of the GRU/IMM-ARCKF is 17.83 meters, which is 39.51meters smaller than the maximum error of IMM-ARCKF algorithm.

Figure (19) is a positioning results in 100s outages. The mean positioning error of GRU/ IMM-ARCKF is 13.72 meters, and that of RBF/ IMM-ARCKF is 24.46 meters. The comparison shows that the performance of GRU network is obviously better than RBF network.

Figure (20) is a positioning results in 100s outages. Because of the long outage time, the error of each algorithm increases continuously. The mean positioning error of the IMM-ARCKF algorithm is as high as 201.86 meters, the mean positioning error of the RBF/IMM-ARCKF is 130.74 meters, while the mean positioning error of the GRU/IMM-ARCKF is only 20.16 meters. It fully embodies the advantage of GRU neural network to assist integrated navigation system after GPS signal loss.

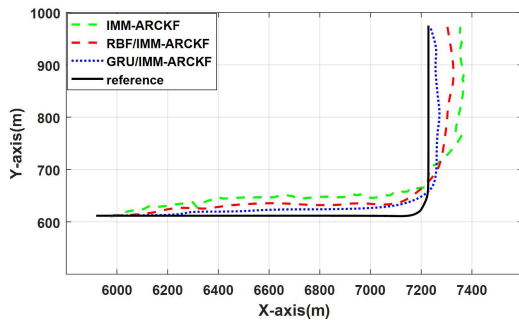


FIGURE 20. Positioning results in 2100s outages.

TABLE 5. Time consumption of different algorithms.

Algorithm	Time(ms)
CKF	11.32
GRU/IMM-ARCKF	19.85

MATLAB 2014 software was used in the simulation experiment. Many simulation experiments were carried out on a portable computer (16G, Intel Core i7-10750H CPU @2.60GHZ), and the running time of the corresponding program was statistically analyzed. Table 5 shows the comparison of calculation time between the two algorithms.

V. CONCLUSION

In this article, IMM-ARCKF algorithm based on GRU is proposed. IMM-ARCKF algorithm mainly solves the uncertainty of system model and noise statistics in the actual system, and improves the robustness and adaptability of the system. GRU neural network can greatly reduce the position error of vehicles in complex urban environment. The performance of GRU/IMM-ARCKF in the case of GPS outages is analyzed. When GPS cannot be properly acquired, the system is in the training stage. The predicted position increment can be obtained by inputting the measurements of specific force, velocity, yaw Angle, and angular velocity into the trained model. After integrating the increment, the predicted GPS position is obtained. Compared with IMM-ARCKF, RBF/IMM-ARCKF and GRU/IMM-ARCKF, the positioning accuracy of GRU/IMM-ARCKF is higher in complex environment. The effectiveness and superiority of the algorithm are proved.

REFERENCES

- [1] S. Godha and M. E. Cannon, "GPS/MEMS INS integrated system for navigation in urban areas," *GPS Solutions*, vol. 11, no. 3, pp. 193–203, May 2007, doi: [10.1007/s10291-006-0050-8](https://doi.org/10.1007/s10291-006-0050-8).
- [2] W. Ding, J. Wang, C. Rizos, and D. Kinlyside, "Improving adaptive Kalman estimation in GPS/INS integration," *J. Navigat.*, vol. 60, no. 3, pp. 517–529, Sep. 2007, doi: [10.1017/S0373463307004316](https://doi.org/10.1017/S0373463307004316).
- [3] H. Nourmohammadi and J. Keighobadi, "Fuzzy adaptive integration scheme for low-cost SINS/GPS navigation system," *Mech. Syst. Signal Process.*, vol. 99, pp. 434–449, Jan. 2018, doi: [10.1016/j.mssp.2017.06.030](https://doi.org/10.1016/j.mssp.2017.06.030).
- [4] R. V. Garcia, P. C. P. M. Pardal, H. K. Kuga, and M. C. Zanardi, "Nonlinear filtering for sequential spacecraft attitude estimation with real data: Cubature Kalman filter, unscented Kalman filter and extended Kalman filter," *Adv. Space Res.*, vol. 63, no. 2, pp. 1038–1050, Jan. 2019, doi: [10.1016/j.asr.2018.10.003](https://doi.org/10.1016/j.asr.2018.10.003).
- [5] K. Reif, S. Gunther, E. Yaz, and R. Unbehauen, "Stochastic stability of the discrete-time extended Kalman filter," *IEEE Trans. Autom. Control*, vol. 44, no. 4, pp. 714–728, Apr. 1999, doi: [10.1109/9.754809](https://doi.org/10.1109/9.754809).
- [6] S. Julier, J. Uhlmann, and H. F. Durrant-Whyte, "A new method for the nonlinear transformation of means and covariances in filters and estimators," *IEEE Trans. Autom. Control*, vol. 45, no. 3, pp. 477–482, Mar. 2000, doi: [10.1109/9.847726](https://doi.org/10.1109/9.847726).
- [7] G. Hu, S. Gao, and Y. Zhong, "A derivative UKF for tightly coupled INS/GPS integrated navigation," *ISA Trans.*, vol. 56, pp. 135–144, May 2015, doi: [10.1016/j.isatra.2014.10.006](https://doi.org/10.1016/j.isatra.2014.10.006).
- [8] I. Arasaratnam and S. Haykin, "Cubature Kalman filters," *IEEE Trans. Autom. Control*, vol. 54, no. 6, pp. 1254–1269, Jun. 2009, doi: [10.1109/TAC.2009.2019800](https://doi.org/10.1109/TAC.2009.2019800).
- [9] I. Arasaratnam, S. Haykin, and T. R. Hurd, "Cubature Kalman filtering for continuous-discrete systems: Theory and simulations," *IEEE Trans. Signal Process.*, vol. 58, no. 10, pp. 4977–4993, Oct. 2010, doi: [10.1109/TSP.2010.2056923](https://doi.org/10.1109/TSP.2010.2056923).
- [10] Y. Zhao, "Performance evaluation of cubature Kalman filter in a GPS/IMU tightly-coupled navigation system," *Signal Process.*, vol. 119, pp. 67–79, Feb. 2016, doi: [10.1016/j.sigpro.2015.07.014](https://doi.org/10.1016/j.sigpro.2015.07.014).
- [11] L. Zhao, J. Wang, T. Yu, H. Jian, and T. Liu, "Design of adaptive robust square-root cubature Kalman filter with noise statistic estimator," *Appl. Math. Comput.*, vol. 256, pp. 352–367, Apr. 2015, doi: [10.1016/j.amc.2014.12.036](https://doi.org/10.1016/j.amc.2014.12.036).
- [12] J. Liu, B.-G. Cai, and J. Wang, "Cooperative localization of connected vehicles: Integrating GNSS with DSRC using a robust cubature Kalman filter," *IEEE Trans. Intell. Transp. Syst.*, vol. 18, no. 8, pp. 2111–2125, Aug. 2017, doi: [10.1109/TITS.2016.2633999](https://doi.org/10.1109/TITS.2016.2633999).
- [13] B. Cui, X. Chen, X. Tang, H. Huang, and X. Liu, "Robust cubature Kalman filter for GNSS/INS with missing observations and colored measurement noise," *ISA Trans.*, vol. 72, pp. 138–146, Jan. 2018, doi: [10.1016/j.isatra.2017.09.019](https://doi.org/10.1016/j.isatra.2017.09.019).
- [14] E. Daeipour and Y. Bar-Shalom, "An interacting multiple model approach for target tracking with glint noise," *IEEE Trans. Aerosp. Electron. Syst.*, vol. 31, no. 2, pp. 706–715, Apr. 1995, doi: [10.1109/7.381918](https://doi.org/10.1109/7.381918).
- [15] E. Mazar, A. Averbuch, Y. Bar-Shalom, and J. Dayan, "Interacting multiple model methods in target tracking: A survey," *IEEE Trans. Aerosp. Electron. Syst.*, vol. 34, no. 1, pp. 103–123, Dec. 1998, doi: [10.1109/7.640267](https://doi.org/10.1109/7.640267).
- [16] X. Tianlai and C. Pingyuan, "Fuzzy adaptive interacting multiple model algorithm for INS/GPS," in *Proc. Int. Conf. Mechatronics Automat.*, 2007, pp. 2963–2967.
- [17] B. Zhu and H. He, "Integrated navigation for Doppler velocity log aided strapdown inertial navigation system based on robust IMM algorithm," *Optik*, vol. 217, Sep. 2020, Art. no. 164871, doi: [10.1016/j.ijleo.2020.164871](https://doi.org/10.1016/j.ijleo.2020.164871).
- [18] E. S. Abdolkarimi and M. R. Mosavi, "Wavelet-adaptive neural subtractive clustering fuzzy inference system to enhance low-cost and high-speed INS/GPS navigation system," *GPS Solutions*, vol. 24, no. 2, Apr. 2020, doi: [10.1007/s10291-020-0951-y](https://doi.org/10.1007/s10291-020-0951-y).
- [19] K.-W. Chiang, A. Noureldin, and N. El-Sheimy, "Multisensor integration using neuron computing for land-vehicle navigation," *GPS Solutions*, vol. 6, no. 4, pp. 209–218, Mar. 2003, doi: [10.1007/s10291-002-0024-4](https://doi.org/10.1007/s10291-002-0024-4).
- [20] A. M. Erkmen, and A. Erkmen, "Enhancing positioning accuracy of GPS/INS system during GPS outages utilizing artificial neural network," *Neural Process. Lett.*, vol. 25, no. 3, pp. 171–186, Jun. 2007, doi: [10.1007/s11063-007-9036-y](https://doi.org/10.1007/s11063-007-9036-y).
- [21] R. Sharaf and A. Noureldin, "Sensor integration for satellite-based vehicular navigation using neural networks," *IEEE Trans. Neural Netw.*, vol. 18, no. 2, pp. 589–594, Mar. 2007, doi: [10.1109/TNN.2006.890811](https://doi.org/10.1109/TNN.2006.890811).
- [22] A. Noureldin, A. El-Shafie, and M. Bayoumi, "GPS/INS integration utilizing dynamic neural networks for vehicular navigation," *Inf. Fusion*, vol. 12, no. 1, pp. 48–57, Jan. 2011, doi: [10.1016/j.inffus.2010.01.003](https://doi.org/10.1016/j.inffus.2010.01.003).
- [23] X. Chen, C. Shen, W.-B. Zhang, M. Tomizuka, Y. Xu, and K. Chiu, "Novel hybrid of strong tracking Kalman filter and wavelet neural network for GPS/INS during GPS outages," *Measurement*, vol. 46, no. 10, pp. 3847–3854, Dec. 2013, doi: [10.1016/j.measurement.2013.07.016](https://doi.org/10.1016/j.measurement.2013.07.016).

- [24] G. Wang, X. Xu, Y. Yao, and J. Tong, "A novel BPNN-based method to overcome the GPS outages for INS/GPS system," *IEEE Access*, vol. 7, pp. 82134–82143, 2019, doi: [10.1109/ACCESS.2019.2922212](https://doi.org/10.1109/ACCESS.2019.2922212).
- [25] C. Shen, Y. Zhang, J. Tang, H. Cao, and J. Liu, "Dual-optimization for a MEMS-INS/GPS system during GPS outages based on the cubature Kalman filter and neural networks," *Mech. Syst. Signal Process.*, vol. 133, Nov. 2019, Art. no. 106222, doi: [10.1016/j.ymssp.2019.07.003](https://doi.org/10.1016/j.ymssp.2019.07.003).
- [26] P. Doostdar, J. Keighobadi, and M. A. Hamed, "INS/GNSS integration using recurrent fuzzy wavelet neural networks," *GPS Solutions*, vol. 24, no. 1, p. 29, Jan. 2020, doi: [10.1007/s10291-019-0942-z](https://doi.org/10.1007/s10291-019-0942-z).
- [27] N. Bonnor, "Principles of GNSS, inertial, and multisensor integrated navigation system," *J. Navigat.*, vol. 67, no. 1, pp. 191–192, Jan. 2014, doi: [10.1017/S0373463313000672](https://doi.org/10.1017/S0373463313000672).
- [28] Z. M. Durovic and B. D. Kovacevic, "Robust estimation with unknown noise statistics," *IEEE Trans. Autom. Control*, vol. 44, no. 6, pp. 1292–1296, Jun. 1999, doi: [10.1109/9.769393](https://doi.org/10.1109/9.769393).
- [29] X. Zhao, J. Li, X. Yan, and S. Ji, "Robust adaptive cubature Kalman filter and its application to ultra-tightly coupled SINS/GPS navigation system," *Sensors*, vol. 18, no. 7, p. 2352, Jul. 2018, doi: [10.3390/s18072352](https://doi.org/10.3390/s18072352).
- [30] W. Fu-Mei and Y. Yuan-xi, "An extended adaptive Kalman filtering in tight coupled GPS/INS integration," *Surv. Rev.*, vol. 42, no. 316, pp. 146–154, Apr. 2010, doi: [10.1179/003962610X12572516251646](https://doi.org/10.1179/003962610X12572516251646).
- [31] A. Graves, A. Mohamed and G. Hinton, "Speech recognition with deep recurrent neural networks," in *Proc. Int. Conf. Acoust. Speech Signal Process.*, 2013, pp. 6645–6649.
- [32] R. Zhao, D. Wang, R. Yan, K. Mao, F. Shen, and J. Wang, "Machine health monitoring using local feature-based gated recurrent unit networks," *IEEE Trans. Ind. Electron.*, vol. 65, no. 2, pp. 1539–1548, Feb. 2018, doi: [10.1109/TIE.2017.2733438](https://doi.org/10.1109/TIE.2017.2733438).
- [33] S. Hochreiter and J. Schmidhuber, "Long short-term memory," *Neural Comput.*, vol. 9, no. 8, pp. 1735–1780, Nov. 1997, doi: [10.1162/neco.1997.9.8.1735](https://doi.org/10.1162/neco.1997.9.8.1735).
- [34] G. Tang, Y. Wu, C. Li, P. K. Wong, Z. Xiao, and X. An, "A novel wind speed interval prediction based on error prediction method," *IEEE Trans. Ind. Informat.*, vol. 16, no. 11, pp. 6806–6815, Nov. 2020, doi: [10.1109/TII.2020.2973413](https://doi.org/10.1109/TII.2020.2973413).



DENGAO LI was born in Shanxi, China, in 1971. He has worked on the projects funded by the National 863 Project and the National Nature Funds. He is currently a Professor with the Taiyuan University of Technology. His research interests include medical signal processing, satellite signal processing, and powerless sensing. He is also the Chair of the ACM Taiyuan Chapter and the Director of the Communication Institute of Shanxi and the Internet Association of Shanxi.



YUQI WU was born in Shanxi, China, in 1995. She is currently pursuing the M.S. degree with the Taiyuan University of Technology. Her research interests include satellite signal processing and GPS/INS integrated navigation systems.



JUMIN ZHAO was born in Shanxi, China, in 1976. She has worked on around the projects funded by the National 863 Project and the National Nature Funds. She is currently a Professor with the Taiyuan University of Technology. Her research interests include cyber-physical systems and weak signal processing. She is a Senior Member of CIE, a member of CIE-YoSC, and a Committee Member of CCF. She is also the Deputy Secretary-General of ACM Taiyuan Chapter.

...